# Molecular Mechanics Analysis of Tet Repressor TRP-43 Fluorescence

Patrizio Silvi Antonini,* Wolfgang Hillen,# Norbert Ettner,# Winfried Hinrichs,§ Piercarlo Fantucci,*
Silvia M. Doglia,¶ Jean-Alain Bousquet,‖ and Marie Chabbert‖

*Dipartimento di Chimica Inorganica and Metallorganica, Università degli Studi di Milano, 20133 Milano, Italy; #Lehrstuhl für Mikrobiologie, Institut für Mikrobiologie, Biochemie und Genetik der Friedrich-Alexander Universität Erlangen-Nürnberg, 91058 Erlangen, Germany; §Institut für Kristallographie, Freie Universität Berlin, 14195 Berlin, Germany; ¶Dipartimento di Fisica, Università degli Studi di Milano, 20133 Milano, Italy; and ‖Laboratoire de Biophysique, Faculté de Pharmacie de l'Université Louis Pasteur de Strasbourg, CNRS URA 491, BP 24, 67401 Illkirch, France

ABSTRACT   A 35% decrease in the fluorescence intensity of F75 TetR Trp-43 was observed upon binding of the tetracycline derivative 5a,6-anhydrotetracycline (AnTc) to the repressor. The fluorescence decay of Trp-43 in F75 TetR and in its complex with AnTc could be described by the sum of three exponential components, with lifetimes of about 6, 3, and 0.3 ns. The amplitudes, however, were markedly altered upon binding. The minimized energy mapping of Trp-43 $\chi_1 \times \chi_2$ isomerization clearly indicated the existence of three main potential wells at positions $(-160°, -90°)$ (rotamer I), $(-170°, 90°)$ (rotamer II), and $(-70, 150°)$ (rotamer III). Our study of Trp-43 environment for each of the three rotamers suggests that the longest decay component may be assigned to rotamer II, the middle-lived component to rotamer I, and the subnanosecond component to rotamer III. The origin of the changes in the rotamer distribution upon AnTc binding is discussed. Anisotropy decays are also discussed within the framework of the rotamer model.

## INTRODUCTION

The tryptophan residue is widely used as an intrinsic fluorescent probe to investigate protein conformation and structural changes. Progress in molecular engineering led to the blooming of single Trp protein mutants, in which a strategically placed Trp can be used as a site-labeling group. The very high sensitivity of the indole moiety to environmental conditions, however, makes the interpretation of Trp fluorescence very difficult in terms of conformation. The indole chromophore has multiple nonradiative decay pathways that depend on environment. The fluorescence decay of tryptophan, whether in proteins and peptides or as a free amino acid, is usually multiexponential (Beechem and Brand, 1985). This multiexponential decay is attributed to the existence of multiple ground-state conformers with distinct microenvironments and thus lifetimes due to differences in proximity of functional groups that quench indole fluorescence (Szabo and Rayner, 1980; Petrich et al., 1983). A better understanding of the parameters determining the fluorescence decay of a Trp residue and its relationship to the protein local structure is clearly required to take full advantage of the high potential yield of information from this residue. Energy mapping of the Trp side-chain $\chi_1$-$\chi_2$ isomerization (Haydock, 1993; Silva and Prendergast, 1996) should be a very efficient method of searching for stable rotamer positions and correlating lifetimes with structural parameters.

Our group has been involved in a detailed spectroscopic investigation of Tet repressor Trp-43 (Chabbert et al., 1992; Peviani et al., 1995). Class B Tet repressor (TetR) controls the transcription of the Tn10-encoded tet genes conferring resistance to tetracycline on Gram-negative bacteria (for a recent review, see Hillen and Berens, 1994). The engineered F75 TetR possesses a single Trp residue (Trp-43) located in the recognition helix of the helix-turn-helix motif (Fig. 1). Because of this strategic position in the operator binding domain, Trp-43 has been used as a spectroscopic probe to investigate the structure of the helix-turn-helix motif (Chabbert et al., 1992) and TetR binding to DNA (Peviani et al., 1995). The recent resolution of the crystal structure of the homologous class D TetR complexed to tetracycline or to 7-chlorotetracycline (Hinrichs et al., 1994; Kisker et al., 1995) prompted us to initiate a study aimed at correlating Trp-43 fluorescence decay with structural parameters. In this report, molecular mechanics and graphics methods are used to understand the time-resolved fluorescence of Trp-43 in the free protein and in the complex with the tetracycline derivative 5a,6-anhydrotetracycline (AnTc). We show that the Trp-43 multiexponential decay can be correlated with the existence of three main rotamers of the Trp side chain and that AnTc binding induces a marked change in the rotamer distribution. The possible origins of this change are discussed. Time-resolved anisotropy data are also discussed within the framework of the rotamer model.

## MATERIALS AND METHODS

### Materials

All the chemicals were of reagent grade or better. 5a,6-Anhydrotetracycline was from Jansen and was used without further purification. Class B F75 TetR was prepared as previously described (Peviani et al., 1995). The protein was stored at 4°C as a precipitate in 60% saturation ammonium
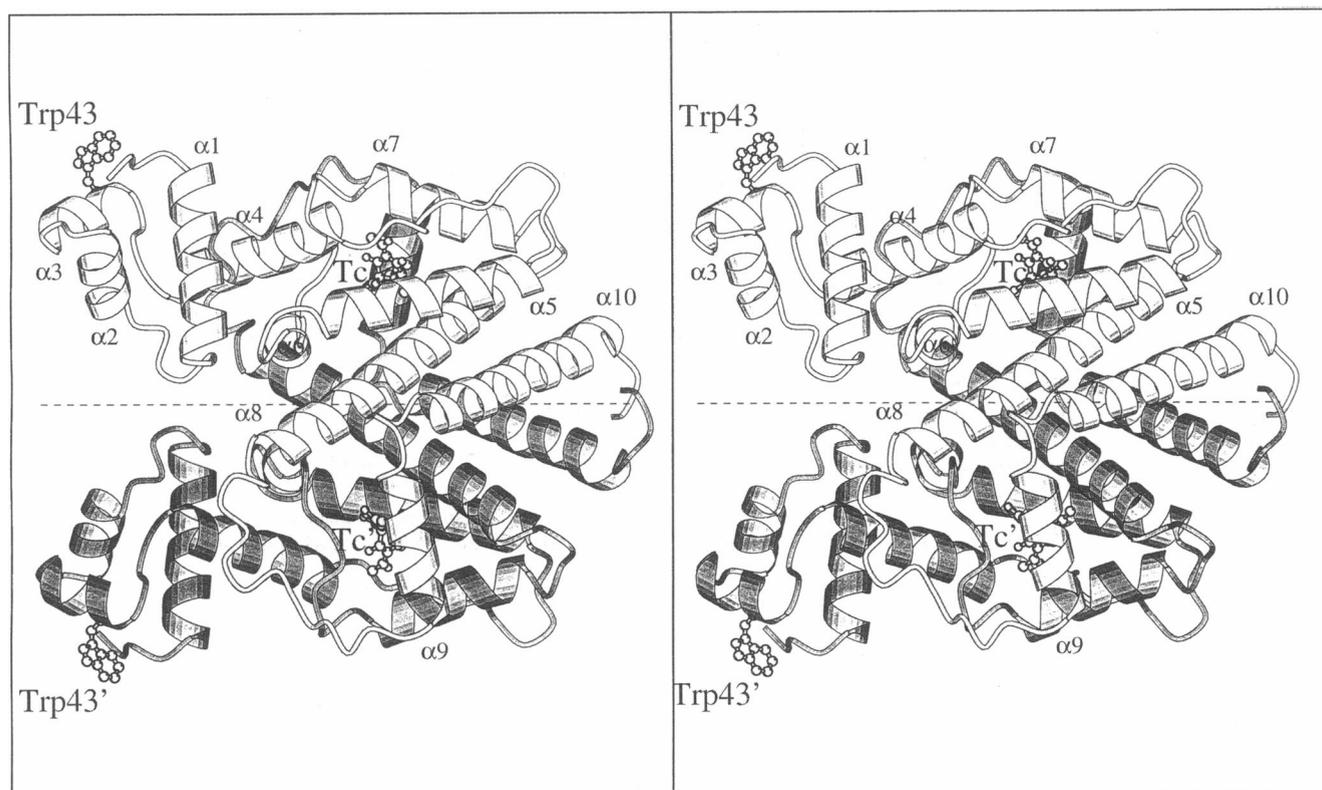
FIGURE 1   Ribbon stereo drawing of TetR (class D) dimer in the complex with $Mg^{2+}$-Tc. Trp-43 and tetracycline are drawn in a ball-and-stick representation. Drawn with MOLSCRIPT.

sulfate. Before measurements, an aliquot was dissolved in 20 mM Tris-HCl (pH 8.0), 200 mM NaCl, 20 mM $\beta$-mercaptoethanol ($\beta$-ME), and buffer exchanged in a PD10 column (Pharmacia). The experiments were carried out in 10 mM Tris (pH 8.0), 100 mM NaCl, 5 mM $MgCl_2$, and 10 mM $\beta$-ME at 20°C.

## Spectroscopic methods

The concentrations were determined spectrophotometrically. Because Trp-43 does not interfere with tetracycline binding (Hansen et al., 1987; see also Fig. 1), the molar extinction coefficient for AnTc bound to F75 TetR was taken equal to that of AnTc bound to the Y43F75 TetR mutant ($11,600 M^{-1} cm^{-1}$ at 430 nm). UV absorption spectra were recorded on a Cary 4 spectrophotometer. Steady-state fluorescence measurements were carried out with a MPF66 spectrofluorometer (Perkin-Elmer). Titrations were carried out by measuring the integrated fluorescence intensity of the Trp fluorescence emission band from 300 up to 400 nm, to avoid the contribution of AnTc fluorescence ranging from 450 to 750 nm. Spectra were corrected for the buffer-only blank contribution, and for the instrumental excitation and emission wavelength dependence, by using built-in correction curves. When the excitation spectra of AnTc bound to F75 TetR and to F43F75 TetR were compared, a 2% change in the signal was taken as the observable limit for significant fluorescence increase at 280 nm due to energy transfer from Trp to AnTc. Taking into account the extinction coefficients of AnTc and Trp-43, this corresponds to an energy transfer efficiency of 12% (Berman et al., 1980).

The Förster distance (in cm) between Trp-43 and AnTc was estimated from

$$R_0^6 = 8.8 \times 10^{-25}(\kappa^2 n^{-4}\phi_d J), \qquad (1)$$

where $\kappa^2$ is the orientation factor (taken to be 2/3), $n$ is the refractive index of the medium (1.4), $\phi_d$ is the quantum yield of the donor, and $J$ is the overlapping integral (in $M^{-1} cm^3$) between the emission spectrum of the donor and the absorption spectrum of the acceptor (Förster, 1948). $\phi_d$ was taken to be 0.12, corresponding to the product of the quantum yield of the protein in the absence of AnTc (0.18) by the relative decrease in the fluorescence intensity upon AnTc binding, under the assumption that most of the fluorescence quenching was not due to energy transfer.

Steady-state anisotropy measurements on AnTc bound to F75 tetR were carried out on a SLM 8000 spectrofluometer (T-format device). The emission wavelength was set at 481 nm with interferential filters.

## Fluorescence lifetime measurements

Fluorescence lifetime measurements were carried out with the pulse fluorometry technique, as described elsewhere (Peviani et al., 1995). The excitation wavelength was 295 nm. The fluorescence emission was observed at the emission maximum wavelength (350 nm) through a 16-nm bandwidth monochromator (Jobin-Yvon). The counting was stopped when the total number of counts reached $8 \times 10^5$ (free F75 TetR) or $7 \times 10^5$ (complex with AnTc). The calibration of the multichannel analyzer was 53 ps/channel. The decay data were analyzed as sums of exponentials:

$$I(t) = \Sigma_i \, \alpha_i e^{-t/\tau_i}, \qquad (2a)$$

with

$$\Sigma_i \, \alpha_i = 1, \qquad (2b)$$

by using an iterative reconvolution procedure based on the Marquardt algorithm. The weighting factors used in the $\chi^2$ test were determined

experimentally from a set of five decays (Lami and Piémont, 1992). This limited number of decays was chosen to avoid photodegradation of the sample (Peviani et al., 1995). The number of exponentials used in the fitting procedure was progressively increased until the fit was judged adequate from the $\chi^2$ value and visual inspection of weighted residuals and autocorrelation factors. Four components were required for an acceptable fit of the decay data. The fourth component (subpicosecond range, weight < 0.2%) arose from a systematic error due to discretization of the instrument response function when the channel width is on the order of the response function full width at half-maximum (Vix and Lami, 1995). This component was thus excluded from the analysis presented here. For comparative data presented in Table 1, measurements were carried out on the same sample. Rigorous error analysis was carried out as described by Beechem (1992). Analysis of the five decays was carried out for a set of fixed lifetime values. The $\chi^2$ value was plotted as a function of the fixed lifetime. The $\chi^2$ increase corresponding to a given confidence interval was determined by the F-statistics (Bevington, 1969).

In the presence of AnTc, the observed lifetimes $\tau_i$ could be corrected for energy transfer to give intrinsic lifetimes $\tau_{i,corr}$:

$$1/\tau_{i,corr} = 1/\tau_i - k_{ET}, \tag{3}$$

where the energy transfer rate $k_{ET}$ is given by (Förster, 1948)

$$k_{ET} = 8.71 \times 10^{23} r^{-6} J \kappa^2 n^{-4} k_r \, s^{-1}. \tag{4}$$

The radiative decay time $k_r$ was assumed to be $4.4 \times 10^7 \, s^{-1}$ from the ratio of the quantum yield to the average lifetime in free repressor, which is similar to that determined for different indole derivatives (Ricci, 1970). Dynamically averaged orientation factors $\langle \kappa^2 \rangle$ were calculated according to the model of Dale et al. (1979). The Trp transition dipole was oriented from the middle of the $C^{\delta2}$-$C^{\epsilon2}$ bond to the middle of the $N^{\epsilon1}$-$C^{\delta1}$ bond, which approximates the $^1L_a$ orientation. The AnTc transition dipoles were oriented along the long and short axes of the BCD chromophore. The axial depolarization factors was 1 for AnTc (rigidly bound to TetR) and was equal to the square root of the generalized order parameter for Trp-43. In spite of segmental motion on the energy transfer time scale, the dynamic averaging regime should give a good estimate for the orientation factor, because the energy transfer efficiency is low (less than 20%) (Dale et al., 1979).

The average lifetime of AnTc was determined by phase fluorometry with an SLM 48000 spectrofluorometer.

## Time-resolved anisotropy measurements

Time-resolved anisotropy measurements were carried out as previously described (Peviani et al., 1995). The fluorescence anisotropy $r(t)$ was obtained by fitting the experimental $I_{parallel}(t)$ decay directly to the anisotropy-containing expression for this fluorescence component (Cross and Fleming, 1984). The $r(t)$ decay was fit as

$$r(t) = \Sigma_i r_i \exp(-t/\theta_i) + r_\infty, \tag{5}$$

where $r_i$ is the amplitude of the rotational correlation time $\theta_i$ and $r_\infty$ is the infinite time anisotropy. The data could be adequately fit by two components, as judged from the $\chi^2$ values and the plots of the residuals. The infinite time anisotropy, $r_\infty$, was not zero. Direct analysis of the anisotropy

decay tail showed the existence of an additional very long rotational correlation time due to overall tumbling of the repressor dimer. However, the limited sensitivity of the analysis did not allow us to recover this motion when the anisotropy decay was analyzed as the sum of exponentials. The anisotropy decay measurements were repeated 10 times on the same sample to determine the sample covariance matrix and to analyze statistically the set of decay parameters obtained (Lami and Piémont, 1992).

Anisotropy data were analyzed according to the model of Clore et al. (1990), who extended the Lipari and Szabo model (Lipari and Szabo, 1980) to the case of two internal motions separated by at least one order of magnitude. The anisotropy decay is approximated by a correlation function that describes internal motions and is treated as a biexponential decay with two time constants for internal motion $\theta_s$ and $\theta_f$:

$$r(t)/r_{t=0} \approx C(t) = S_s^2 S_f^2 + S_f^2 (1 - S_s^2) \exp(-t/\theta_s) \tag{6}$$
$$+ (1 - S_f^2) \exp(-t/\theta_f).$$

The slower and faster motions are characterized by order parameters $S_s^2$ and $S_f^2$. Comparison of Eq. 5 with $i = 2$ and Eq. 6 shows that

$$r_{t=0} = r_1 + r_2 + r_\infty \tag{7}$$

$$S_f^2 = (r_2 + r_\infty)/r_{t=0} \tag{8}$$

$$S_s^2 = r_\infty/(r_2 + r_\infty). \tag{9}$$

In the wobbling-in-a-cone model of Lipari and Szabo (1980), the order parameter of the probe is related to the semiangle $\theta$ of the cone, in which it freely diffuses by the relationship

$$S = \cos \theta (1 + \cos \theta)/2. \tag{10}$$

The generalized order parameter is equal to $S^2 = r_\infty/r_0$.

## Molecular mechanics

The $\chi_1 \times \chi_2$ energy mapping was performed with the Discover (94.0 version) program from INSIGHT II (BIOSYM Technologies) on an Indigo[2] workstation (Silicon Graphics), using the coordinates of the homologous class D TetR in the complex with tetracycline (Hinrichs et al., 1994). The DNA binding domain is highly conserved between the two repressor classes, with a single type conserved mutation at position 36. There is no mutation in the vicinity of Trp-43. Consequently, we used the coordinates of the class D protein truncated at residue 48 (included) without further modification. This N-terminal part of the protein included helices 1–3 and the turn between helices 3 and 4 (Fig. 1). Adiabatic mapping was conducted by 10° increment rotation of Trp-43 about the side-chain torsion angles and subsequent energy minimization using the Consistent Valence Forcefield (CVFF) (Dauber-Osguthorpe et al., 1988). During minimization, only the side chains of residues near Trp-43 (Pro-39, Thr-40, Tyr-42, His-44 and Lys-46) and the constrained Trp-43 side chain itself were allowed to conformationally relax. The minimization procedure at each Trp dihedral point used the steepest descent method when the maximum energy derivative was greater than 1000 kcal·mol$^{-1}$ · Å$^{-1}$, followed by the con-

**TABLE 1 Multiexponential analysis of typical Trp-43 fluorescence decay in free F75 TetR and in the complex with AnTc\***

| | $\tau_1$ (ns) | $\alpha_1$ | $\tau_2$ (ns) | $\alpha_2$ | $\tau_3$ (ns) | $\alpha_3$ | $\chi^2$ |
|---|---|---|---|---|---|---|---|
| −AnTc | $6.74 \pm 0.14$ | $0.435 \pm 0.022$ | $2.78 \pm 0.09$ | $0.386 \pm 0.031$ | $0.24 \pm 0.04$ | $0.179 \pm 0.021$ | 1.13 |
| +AnTc | $5.47 \pm 0.25$ | $0.272 \pm 0.036$ | $2.64 \pm 0.15$ | $0.592 \pm 0.036$ | $0.28 \pm 0.02$ | $0.136 \pm 0.019$ | 1.29 |

\*Measurements were carried out in a buffer containing 10 mM Tris (pH 8.0), 100 mM NaCl, 5 mM MgCl$_2$, 10 mM βME. The emission wavelength was 350 nm. The decay data correspond to the means ($\pm$SE) of five measurements on the same sample. The F75 TetR dimer concentration was 1 μM. When AnTc was present, its concentration was 2 μM.

jugate gradient method until the maximum energy derivative met the convergence criterion of 0.1 kcal $\cdot$ mol$^{-1}$ $\cdot$ Å$^{-1}$. No cutoff was used for nonbonded interactions. Simulations were done in vacuum. The maximum number of iterations (1000) was high enough to ensure that the convergence criterion was always reached, avoiding addition of stress during mapping. Examination of starting ($\chi_1 = -180°$) and final ($\chi_1 = 180°$) structures showed that a secondary transition with conformational rearrangement of the Thr-40 $O^{\gamma 1}$-$H^{\gamma 1}$ group occurred during mapping. This secondary transition led to a constant energy shift of $-1.0$ kcal/mol in the *trans* rotamer area, as there is only weak interaction between Thr-40 and Trp-43 side chains. It was avoided by skipping the step in which it occurred in the mapping process. In spite of this problem, adiabatic mapping was preferred to minimum perturbation mapping (Haydock, 1993), because, with this latter method, we obtained totally aberrant structures in the case of strong initial overlap. We did not observe aberrant structures during adiabatic mapping. We checked that the two methods gave identical results in the useful part of the map ($-180° < \chi_1 < -60°$).

The normalized Boltzmann population, $P(\chi_1, \chi_2)$, of the ($\chi_1, \chi_2$) isomeric position was computed from the potential energy surface:

$$P(\chi_1, \chi_2)$$
$$= \exp(-E(\chi_1, \chi_2)/RT)/(\Sigma_i \Sigma_j \exp(-E(\chi_{1i}, \chi_{2j})/RT)), \tag{11}$$

where $R$ is the ideal gas constant, $T$ is the temperature, and $E(\chi_{1i}, \chi_{2j})$ is the potential energy at position ($\chi_{1i}, \chi_{2j}$). The population fraction of each rotamer was obtained by integration over the corresponding area.

The graphic analyses were performed using the INSIGHT II molecular modeling package. The dihedral angles $\chi_1$ and $\chi_2$ are defined by the bond connectivities N-$C^\alpha$-$C^\beta$-$C^\gamma$ and $C^\alpha$-$C^\beta$-$C^\gamma$-$C^{\delta 2}$, respectively. Our rotamer definitions are the same as those of Ponder and Richards (1987). The $g^+$ and $g^-$ rotamers correspond to $\chi_1$ angles between 0° and 120° and 0° and $-120°$, respectively. The *trans* rotamer corresponds to a $\chi_1$ angle between $-120°$ and 120°. The perpendicular and antiperpendicular rotamers correspond to $\chi_2$ angles between 0° and 180° and 0° and $-180°$, respectively.

## RESULTS

### Steady-state fluorescence

Because of the very efficient resonance energy transfer from tryptophan to tetracycline (Takahashi et al., 1986), understanding Trp-43 fluorescence in the presence of tetracycline is not straightforward. To overcome this problem, we have investigated the spectroscopic changes of Trp-43 upon TetR binding to anhydrotetracycline. The lowest absorption band of this tetracycline derivative is about 100 nm red shifted as compared to tetracycline, leading to a marked decrease in the overlapping integral between AnTc absorption and tryptophan emission spectra (Fig. 2 *a*). The AnTc absorption band at 450 nm can be assigned to the $^1A \rightarrow {}^1L_b$ transition of the BCD chromophore, whereas the shoulder at 335 nm can be assigned to the $^1A \rightarrow {}^1L_a$ transition (Machado et al., 1995). The band at 277 nm contains contributions from both the A and BCD chromophores (Schnarr et al., 1979).

The association constant of AnTc to wild-type TetR is on the order of $10^{11}$ M$^{-1}$ (Degenkolb et al., 1991). The association constant of AnTc to F75 TetR is expected to be on the same order of magnitude, as the replacement of Trp-75 by Phe results in a slight stabilization of the TetR-tetracycline complex (Hansen et al., 1987). Fig. 2 *a* displays the steady-state fluorescence spectra of Trp-43 in free F75 TetR
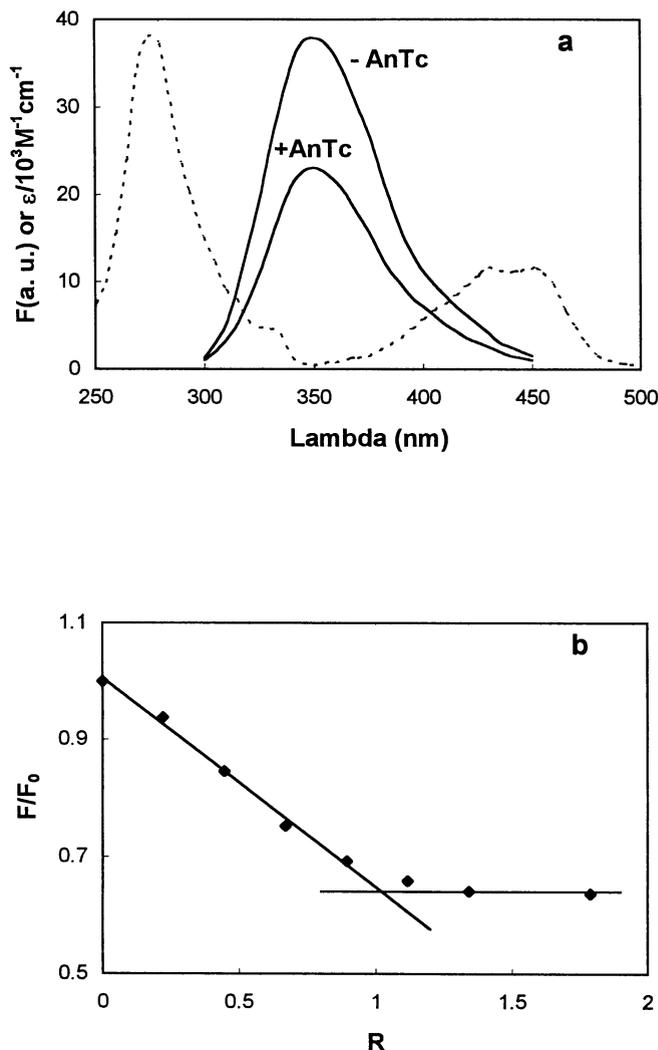
FIGURE 2   (*a*) Steady-state fluorescence spectra of Trp-43 in F75 TetR free and complexed with AnTc. The excitation wavelength was 295 nm. The F75 TetR dimer concentration was 1 $\mu$M. When present, the AnTc concentration was 2 $\mu$M. On the same graph is reported the molar extinction coefficient of AnTc bound to F75 TetR as a function of the wavelength (– – –). (*b*) Titration of F75 TetR by AnTc. $F/F_0$ represents the relative fluorescence intensity decrease and $R$ the molar ratio of AnTc to F75 TetR (in monomers). Measurements were carried out with a F75 TetR dimer concentration of 1 $\mu$M. The straight lines represent the linear best fit of the data (up to $R = 0.8$) and the plateau reached. The buffer used was 10 mM Tris (pH 8.0), 100 mM NaCl, 5 mM Mg$^{2+}$, 10 mM $\beta$-ME.

and in the complex with anhydrotetracycline upon excitation at 295 nm. At this wavelength there is selective excitation of Trp-43 and of anhydrotetracycline, when present, without contribution from TetR tyrosines. The fluorescence emission of AnTc, the quantum yield of which increased 20-fold upon repressor binding, ranged from 450 to 750 nm and was clearly separated from that of Trp-43 (not shown). Binding of anhydrotetracycline to F75 TetR induced a 35% decrease in Trp-43 fluorescence intensity. The emission maximum of Trp-43 was not significantly shifted (350 ± 1 nm in both cases), suggesting that the accessibility to the solvent was not changed upon AnTc binding. The stoichi-

ometry of the complex could be determined by monitoring the decrease in Trp-43 fluorescence intensity as a function of the molar ratio of AnTc to Tet repressor (Fig. 2 b). The changes were proportional to the molar ratio of AnTc to F75 TetR monomer until this ratio was equal to 1. Above this value, a plateau was reached. These results are consistent with the expected 1:1 stoichiometry of the binding and an association constant larger than $10^7$ $M^{-1}$. The anisotropy of AnTc bound to F75 TetR upon excitation at $\lambda_{exc} \geq 400$ nm was 0.31. The limit anisotropy of AnTc in a diethylether/isopentane/ethanol glass (5/5/2) at 100 K was 0.36. Taking into account the repressor rotational correlation time (about 20 ns) and the average lifetime of AnTc bound to F75 TetR (3.1 ns), this indicates that AnTc is rigidly bound to the protein, which is consistent with the very tight tetracycline binding site observed in the crystal structure of the complex (Hinrichs et al., 1994; Kisker et al., 1995).

The changes in the fluorescence intensity of Trp-43 could be due, at least in part, to fluorescence resonance energy transfer from Trp-43 to AnTc. There was no significant difference between the excitation spectra of AnTc bound to F75 TetR and to the double mutant F43F75 TetR, which does not possess Trp residues (Hansen et al., 1987) (not shown). This indicates that the efficiency of energy transfer from Trp-43 to AnTc was lower than 12% (see Materials and Methods). The Förster distance for energy transfer between the two chromophores, estimated from Eq. 1, is 21.4 Å. In the x-ray structure of the complex with tetracycline, the distance between the geometric center of the indole moiety and that of the closest tetracycline BCD chromophore (same monomer) is 31.9 Å. This leads to an energy transfer efficiency of 8%, consistent with the absence of significant AnTc fluorescence sensitization.

## Time-resolved measurements

The fluorescence decay of Trp-43 in F75 TetR alone or in the complex with AnTc could be adequately fit by triple-exponential functions (Table 1). Upon AnTc binding, the longest lifetime decreased from 6.74 to 5.47 ns, whereas the middle and short-lived lifetimes were not significantly altered. The preexponential factor of the longest component decreased from 0.43 to 0.27, whereas the preexponential factor of the middle-lived component concomitantly increased from 0.39 to 0.59. The 20% decrease in the preexponential factor of the subnanosecond component, from 0.18 to 0.14, was not very significant. Because of the possibility of correlated changes between lifetimes and amplitudes in multiexponential decay analysis, rigorous error analysis was carried out as described in Materials and Methods. Fig. 3 shows confidence interval plots on the recovered lifetimes. Analysis corresponding to the 90% confidence level are summarized in Table 3. Within the 90% confidence level limit, the preexponential term of the long component decreased from the 0.40–0.50 range to the 0.18–0.36 range upon anhydrotetracycline binding,

whereas that of the middle-lived component increased from the 0.32–0.43 range to the 0.51–0.68 range. The subnano-second preexponential factor decreased slightly from the 0.15–0.18 range to the 0.13–0.15 range. This clearly indicates that the marked changes observed in preexponential factors of the longest two components upon AnTc binding are not related to artefactual correlation between decay parameters, but have a physical meaning.

The energy transfer contribution should be estimated to determine whether the significant decrease in the longest lifetime upon AnTc binding is due to an intrinsic change in nonradiative decay rate or is a result of energy transfer from Trp to AnTc. Anisotropy measurements (see below) indicate large amplitude motion of Trp-43 with a generalized order parameter of 0.12. Within the framework of the rotamer model, which makes it possible to assign each decay component to a Trp rotamer (see Discussion), we could calculate the dynamically averaged values of the orientation factors $\langle \kappa^2 \rangle$ for two perpendicular orientations of the acceptor dipole within the anhydrotetracycline BCD plane (main acceptor) by using the model proposed by Dale et al. (1979). Table 3 indicates that rotational averaging leads to quite precise estimates of $\langle \kappa^2 \rangle$ for the three main Trp rotamers, regardless of the orientation of the transition dipoles in the BCD plane. By using the lifetime assignment which will be presented in the Discussion, correction for energy transfer of the three decay components can be carried out. As can be seen from Table 3, the subnanosecond lifetime is not significantly altered by energy transfer. Energy transfer affects the intermediate and long lifetimes by about 5% and 10%, respectively. The corrected lifetime value for the long component is about 6.1 ns. This is significantly lower than the minimum limit at the 90% confidence level (6.4 ns). This indicates about an 20% increase in the nonradiative decay rate of this component upon AnTc binding. The other two lifetimes are not significantly altered by AnTc binding. It is noteworthy, however, that the same absolute change in the nonradiative decay rates ($2 \times 10^7$ $s^{-1}$) of the shortest two components would not lead to significant changes in their lifetimes.

## Anisotropy measurements

Time-resolved anisotropy data were analyzed using a non-associative model, i.e., the correlation rotational times were not associated with a fluorescence decay component, but with the overall fluorescence decay. Table 4 shows typical analysis and indicates that there are no significant changes in the anisotropy decay upon AnTc binding. The anisotropy decay data could be described by the sum of two exponential components with clearly distinct time scales, as previously observed at low ionic concentration (Peviani et al., 1995). The initial anisotropy $r_{t=0}$, equal to $\Sigma r_i + r_\infty$, was 0.200 ± 0.001 in both cases. This value is markedly lower than 0.27, the limit anisotropy of Trp-43 at the same exci-
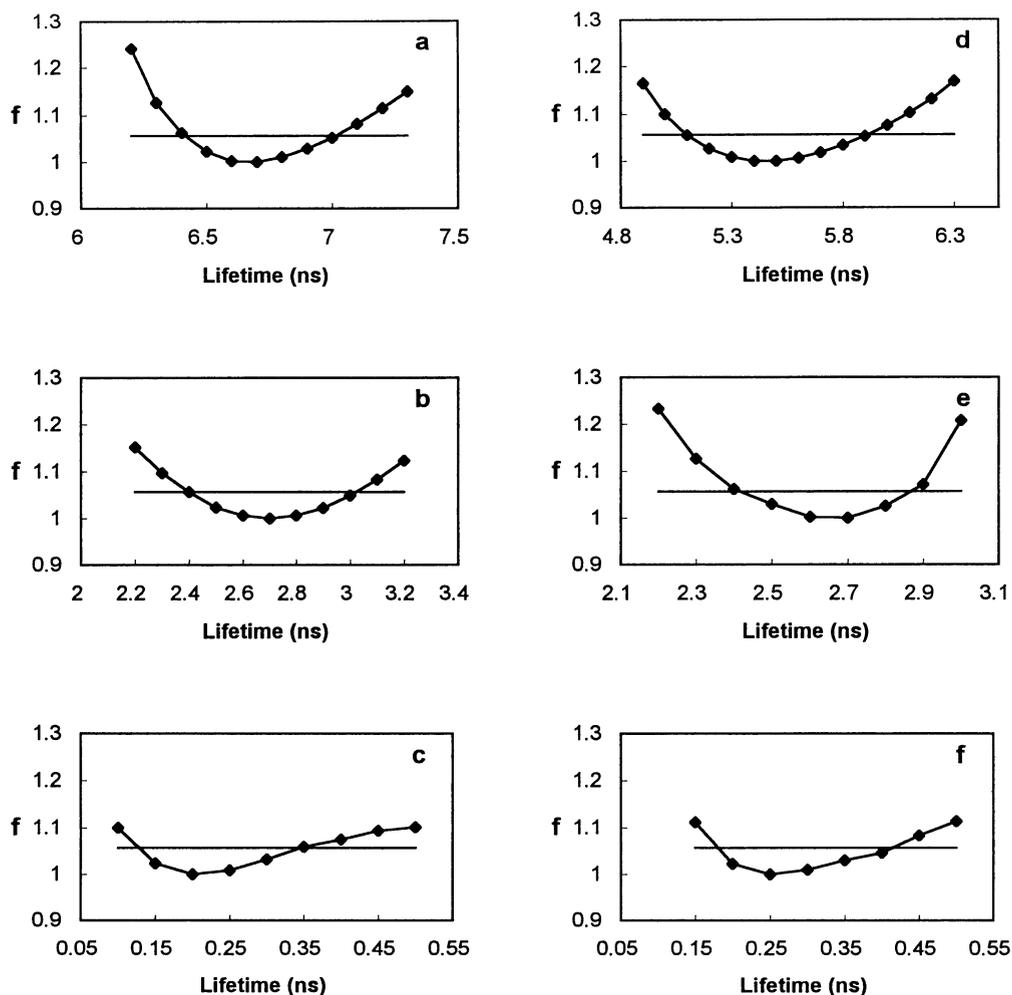
FIGURE 3   Confidence interval plots for the three lifetimes recovered from the multiexponential analysis of Trp-43 decay with one fixed lifetime in TetR free ($a$–$c$) or complexed with AnTc ($d$–$f$). $f$ represents the ratio $\chi^2/\chi^2_{min}$. The horizontal lines represent the 90% confidence level. The actual confidence limits are reported in Table 2.

tation and emission wavelength ($r_0$) (Chabbert et al., 1992). This indicates the existence of a picosecond/subpicosecond rotational motion that is too fast to be observable by our

**TABLE 2   Rigorous error analysis***

|        | $\tau_1$ (ns) | $\tau_2$ (ns) | $\tau_3$ (ns) | $\alpha_1$ | $\alpha_2$ | $\alpha_3$ |
|--------|--------|--------|--------|--------|--------|--------|
| $-$AnTc | **6.40** | 2.46 | 0.22 | 0.501 | 0.338 | 0.161 |
|        | **7.00** | 2.98 | 0.26 | 0.397 | 0.427 | 0.176 |
|        | 6.39 | **2.40** | 0.20 | 0.492 | 0.325 | 0.182 |
|        | 7.00 | **3.00** | 0.27 | 0.397 | 0.429 | 0.174 |
|        | 6.40 | 2.33 | **0.13** | 0.470 | 0.318 | 0.212 |
|        | 6.96 | 3.02 | **0.35** | 0.414 | 0.431 | 0.154 |
| $+$AnTc | **5.10** | 2.48 | 0.25 | 0.337 | 0.531 | 0.132 |
|        | **5.90** | 2.79 | 0.31 | 0.210 | 0.650 | 0.141 |
|        | 5.01 | **2.40** | 0.24 | 0.362 | 0.511 | 0.126 |
|        | 6.16 | **2.90** | 0.33 | 0.178 | 0.676 | 0.146 |
|        | 5.14 | 2.43 | **0.18** | 0.328 | 0.524 | 0.148 |
|        | 5.83 | 2.84 | **0.42** | 0.217 | 0.649 | 0.134 |

*Analysis corresponding to the 90% confidence limits, determined from the plots drawn in Fig. 3. Fixed lifetimes are indicated in bold characters.

device ($\theta_{uf} < 50$ ps). This ultrafast motional process can be attributed to librational motion of Trp-43 about the $C^\alpha$-$C^\beta$ and $C^\beta$-$C^\gamma$ bonds, which occur on the picosecond time scale (Ichiye and Karplus, 1983). This motion is characterized by an order parameter $S^2_{uf}$ (Lipari and Szabo, 1980)

$$S^2_{uf} = r_{t=0}/r_0 \qquad (11)$$

**TABLE 3   Energy transfer corrected lifetimes***

| Rotamer | $\langle \kappa^2_{\|} \rangle$ | $\langle \kappa_\perp \rangle$ | $\tau_i$ (ns) | $\tau_{i,corr\|}$ | $\tau_{i,corr\perp}$ |
|---------|------|------|------|------|------|
| I | 0.35 | 0.41 | 2.64 | 2.76 | 2.78 |
| II | 0.40 | 0.50 | 5.47 | 5.99 | 6.14 |
| III | 0.48 | 0.65 | 0.28 | 0.281 | 0.281 |

*Dynamically averaged orientation factors $\langle \kappa^2_{\|} \rangle$ and $\langle \kappa_\perp \rangle$ were determined for acceptor transition dipoles oriented along the long and short axes of the AnTc BCD chromophore, respectively, using the repressor crystal coordinates and the rotamer positions determined in the text. Energy transfer corrected lifetimes, $\tau_{i,corr\|}$ and $\tau_{i,corr\perp}$, were calculated according to Eqs. 3 and 4, using the dynamically averaged orientation factors $\langle \kappa^2_{\|} \rangle$ and $\langle \kappa^2_\perp \rangle$.

**TABLE 4 Parameters describing Trp-43 anisotropy decay in free F75 TetR and in the complex with AnTc***

| | $\theta_1$ (ns) | $r_1$ | $\theta_2$ (ns) | $r_2$ | $r_\infty$ | $S_{uf}^2$ | $S_f^2$ | $S_s^2$ |
|---|---|---|---|---|---|---|---|---|
| $-$AnTc | $0.18 \pm 0.08$ | $0.041 \pm 0.010$ | $3.6 \pm 0.3$ | $0.131 \pm 0.004$ | $0.028 \pm 0.004$ | $0.74 \pm 0.04$ | $0.80 \pm 0.07$ | $0.18 \pm 0.03$ |
| $+$AnTc | $0.27 \pm 0.13$ | $0.033 \pm 0.022$ | $3.3 \pm 0.2$ | $0.129 \pm 0.004$ | $0.037 \pm 0.003$ | $0.74 \pm 0.04$ | $0.83 \pm 0.07$ | $0.22 \pm 0.02$ |

*Measurements have been carried out in 10 mM Tris (pH 8.0), 100 mM NaCl, 5 mM MgCl$_2$, 10 mM $\beta$-ME. The emission wavelength was 350 nm. The F75 TetR dimer concentration was 1 $\mu$M and that of AnTc, when present, was 2 $\mu$M. The time-resolved anisotropy data correspond to the means ($\pm$SE) of 10 measurements on the same sample. $S_{uf}^2$, $S_s^2$, and $S_s^2$ are the order parameters of the ultrafast (picosecond), fast (subnanosecond), and slow (nanosecond) motions.

equal to 0.74. If the indole moiety moves only about the $C^\beta$-$C^\gamma$ bond, the diffusion angle about this bond can be easily calculated from the order parameter (Weaver et al., 1989):

$$S_{uf}^2 = 1/4(3\cos^2\theta_0 - 1)^2 + 3[(\sin\theta_0 \cos\theta_0 \sin\gamma_2)/\gamma_2]^2$$
$$+ 3/16[(\sin^2\theta_0\sin 2\gamma_2)/\gamma_2]^2, \tag{12}$$

where $\theta_0$ is the angle between the $C^\beta$-$C^\gamma$ bond and the probe dipole. Assuming an angle of $-38°$ between the long axis of the indole moiety and the $^1L_a$ dipole (Yamamoto and Tanaka, 1972), the observed order parameter, 0.74, corresponds to a diffusion angle of $\pm34°$ about the $C^\beta$-$C^\gamma$ bond. Any additional motion about the $C^\alpha$-$C^\beta$ bond will lead to a smaller diffusion angle about the $C^\beta$-$C^\gamma$ bond for a given $S_{uf}^2$. The diffusion angle of $34°$ about the $C^\beta$-$C^\gamma$ bond can thus be considered a limit value that is consistent with the amplitude of the librational motion about the $C^\alpha$-$C^\beta$ and $C^\beta$-$C^\gamma$ bonds estimated from molecular dynamics computations (Ichiye and Karplus, 1983).

In addition to librational motion about the $C^\alpha$-$C^\beta$ and $C^\beta$-$C^\gamma$ bonds, wobbling of these axis occurs because of the flexibility of the protein backbone (Lipari and Szabo, 1982). From NMR measurements, the time scale of backbone motion can vary from less than 50 ps for highly restricted motion (e.g., myosin light chain kinase peptide bound to calmodulin; Chen et al., 1993) to more than 0.5 ns for large-scale segmental motion (e.g., denatured staphylococcal nuclease; Alexandrescu and Shortle, 1994). The sub-nanosecond rotational correlation time could be attributed to this wobbling motion. It is characterized by an order parameter $S_f^2$ of 0.81 $\pm$ 0.02. This corresponds to the wobbling in a cone of semiangle 21 $\pm$ 1° and indicates a restricted flexibility of the protein backbone, consistent with an $\alpha$-helix structure (Mandel et al., 1995).

The longest rotational correlation time of about 3.5 ns was attributed to segmental mobility of the DNA-binding domain. From the relationship between the rotational correlation time, the order parameter (0.20 $\pm$ 0.02), and the wobbling diffusion constant (Lipari and Szabo, 1980), the diffusion constant is equal to 0.055 $\pm$ 0.005 ns$^{-1}$ and corresponds to that of a hydrated sphere of molecular mass 7500 Da. This correlates well with the molecular weight of the TetR N-terminal domain from residues 2 to 63 at the end of helix 4 (7000 Da) (Fig. 1) and indicates that the DNA-binding domain has significant mobility relative to the core

of the protein, which might be important for proper positioning upon operator binding.

## Molecular mechanics investigation

The most popular interpretation of Trp multiexponential decay is the rotamer model (see Discussion). In the crystal structure of TetR, the rotameric orientation of Trp-43 is stabilized by a H bond between Trp-43:N$^{\epsilon 1}$ and Ser-192:O$^{\gamma 1}$ of the neighboring TetR dimer. To investigate the possibility of other stable rotamer positions, we carried out an energy mapping of Trp-43 $\chi_1 \times \chi_2$ isomerization with free-moving neighbors (see Materials and Methods). Fig. 4 clearly indicates the existence of four potential wells corresponding to possible rotamers, within 3 kcal/mol. Table 5 reports their normalized Boltzmann population at 293K. The rotamer position at $(\chi_1, \chi_2) = (-160°, -90°)$ (rotamer I) corresponds to the crystallographic orientation of the Trp-43 indole ring $(-172.9°, -83.6°)$. The energy of rotamer II at $(\chi_1, \chi_2) = (-170°, +90°)$ is 1.4 kcal/mol larger than that of rotamer I. These rotamers correspond to the two perpendicular and antiperpendicular trans Trp rotamers (Schrauber et al., 1993). Rotamer III at $(\chi_1, \chi_2) = (-70°, 150°)$, the energy of which is similar to that of rotamer I, corresponds to the perpendicular g$^-$ rotamer. Rotamer IV has a significantly higher energy (2.4 kcal/mol) and a marginal weight (1%). The energy for $0 < \chi_1 < 120$ is at least 10 kcal/mol, making the g+ rotamers very unlikely.

Fig. 5 shows the environment of Trp-43 for the four rotamers. Rotamers I and II point toward the solvent, whereas rotamers III and IV lie on the protein surface. Rotamers I and II differ mainly with respect to His-44. In rotamer I, the indole and imidazole rings are in van der Waals contacts. The rings have a tilted orientation, with an angle between them of 41°. The closest bonds (Trp43 C$^{\epsilon 3}$-C$^{\zeta 3}$ and His-44 N$^{\delta 1}$-C$^{\epsilon 1}$) are perpendicular. Aromatic residues and histidine can interact whether His is charged or not (Loewenthal et al., 1992; Armstrong et al., 1993). An interaction similar to the Trp-43-His-44 interaction has been observed in barnase, where His-18 stabilizes the protein via a tertiary interaction with Trp-94 (Loewenthal et al., 1992). The potential energy increase preventing rotation of rotamer I about the $C^\alpha$-$C^\beta$ bond at $-180°$ is due to short-range repulsion between the Trp and His rings in van der Waals contact. His-44 itself is stuck between the Trp ring and the carbonyl oxygen of Leu-4, which restricts its mobility.
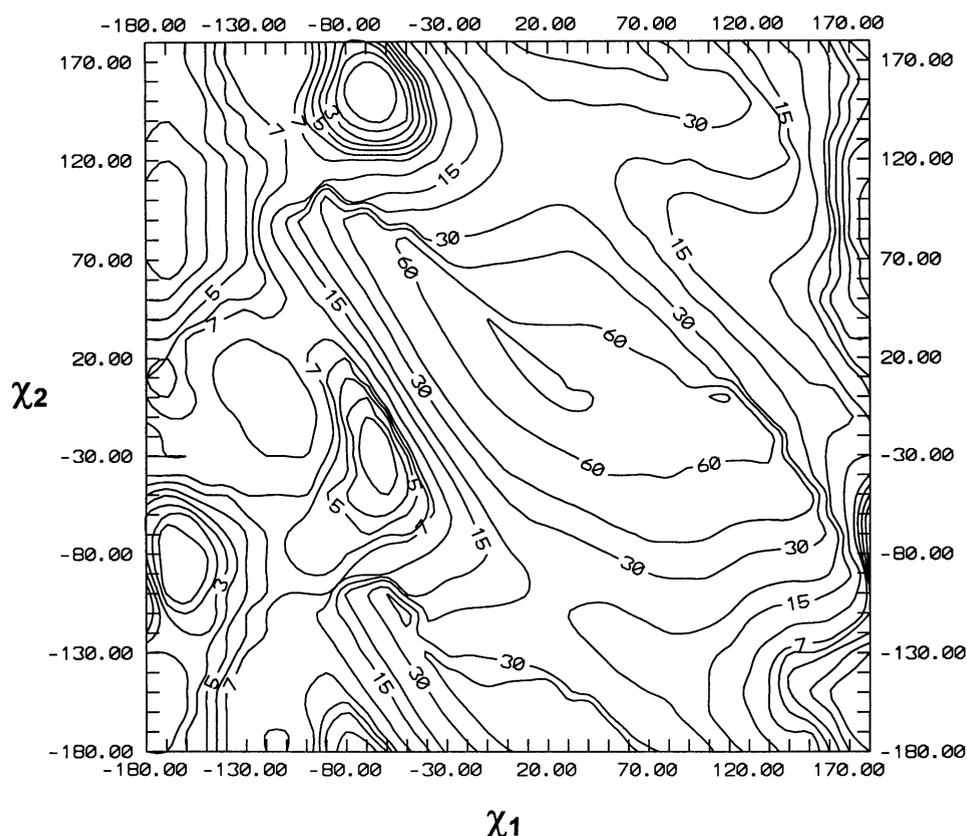
FIGURE 4 Minimized energy mapping of Trp-43 $\chi_1 \times \chi_2$ isomerization. Zero corresponds to the minimum energy of the map. The contour levels are 1, 2, 3, 4, 5, 6, 7, 10, 15, 20, 30, 40, 60, and 80 kcal/mol.

Vicinity of His-44 limits the librational motion of Trp-43 rotamer I, leading to a well more narrow than that of rotamer II (Fig. 4). Rotamer II is too far away from His-44 for specific interaction. Its large potential well corroborates the absence of steric constraints. Rotamer III is in van der Waals contact with the carbonyl oxygen of Pro-39 and the side chain of Thr-40. Rotamer IV is also in van der Waals contact with Pro-39:O and lies near Pro-39:$C^\beta$ and Thr-40: $C^\alpha$. For both rotamers III and IV, librational motion of the indole ring leads to a collisional encounter with Pro-39 and/or Thr-40. This restricts the mobility of these rotamers and leads to narrow wells.

## DISCUSSION

### Lifetime assignment

The origin of the Trp multiexponential decay has been widely investigated during the past 10 years. In spite of

**TABLE 5   Relative populations of the Trp-43 rotamers***

| Rotamer | $\chi_1$ | $\chi_2$ | $E$ (kcal/mol) | $\omega$ |
|---------|----------|----------|----------------|----------|
| I       | −160     | −90      | 0.05           | 0.50     |
| II      | −170     | 90       | 1.42           | 0.10     |
| III     | −70      | 150      | 0              | 0.40     |
| IV      | −60      | −30      | 2.40           | 0.01     |

The minimum energy $E$ of each potential well is given relative to the absolute minimum energy of the map. The relative population $\omega$ of each rotamer is calculated as described in Materials and Methods, with $T = 293$ K.

alternative models such as distribution of lifetimes (Alcala et al., 1987) or transfer of energy model (Bajzer and Prendergast, 1993), the Trp multiexponential decay is usually attributed to the existence of multiple ground-sate conformers of the Trp residue. In the so-called rotamer model, the Trp side chain may adopt low energy conformations because of the rotation about the $C^\alpha$-$C^\beta$ and/or the $C^\beta$-$C^\gamma$ bonds. Each conformation has a different microenvironment, yielding to a distinct nonradiative decay rate due to a different proximity and orientation to quencher groups (Szabo and Rayner, 1980; Petrich et al., 1983). The existence of stable Trp rotamers has been observed by NMR (Skrabal et al., 1979; Dezube et al., 1981). The fluorescence decay of individual Trp rotamers in supersonic jets is monoexponential (Phillips et al., 1988). In a few cases it has been possible to correlate rotamers observed by NMR and lifetime components, for either indole derivatives (Colucci et al., 1990) or Trp in peptide (Ross et al., 1992). A recent study of Trp fluorescence decay in a protein crystal corroborates the rotamer model (Dahms et al., 1995).

The fluorescence decay of F75 TetR Trp-43 is consistent with a model in which fluorescence arises from three discrete emitting species, the equilibrium of which is altered upon AnTc binding. The energy mapping of Trp-43 $\chi_1 \times \chi_2$ isomerization (Fig. 4) was done to find possible low-energy conformations for the Trp-43 side chain. It clearly indicates the existence of three main potential wells corresponding to possible discrete rotamers of Trp-43. A fourth rotamer, albeit possible, should be marginal, as its probability is an

FIGURE 5    Stereo view of Trp-43 environment for rotamers I (*a*), II (*b*), III (*c*), and IV (*d*), showing Leu-4, Pro-39, Thr-40, Leu-41, Tyr-42, Trp-43, His-44, Val-45, and Lys-46. The helix-3 axis is perpendicular to the drawing. The dotted surfaces correspond to the van der Waals surfaces of the Trp-43 and His-44 rings and of the oxygen atoms of Pro-39 and Leu-4. The N- and C-terminal atoms of Leu-4 and of the sequence 39–46 are indicated for the purpose of clarity.

order of magnitude lower than that of the other rotamers. This strongly suggests that the three lifetimes can be correlated to the three main rotamers of Trp-43 and corroborates the "rotamer" model for the interpretation of fluorescence decay data.

The environment of the three main rotamers has thus been investigated to assign the lifetimes to the different rotamers. Trp nonradiative decay pathways that are sensitive to environment are excited-state electron and proton transfers and solvent quenching (Yu et al., 1992, 1995; Chen et al., 1996). Charge transfer from the excited indole

moiety to the carbonyl group of the peptide bond (Ricci and Nesta, 1976; Werner and Forster, 1979; Petrich et al., 1983; Chen et al., 1996) is probably the main nonradiative pathway of Trp decay in protein. The electrophilicity of this amide carbonyl within a peptidic chain is increased enough to allow efficient electron transfer. Another possible quenching process is excited-state proton transfer from a strong proton donor to an adjacent aromatic carbon of the indole moiety (Yu et al., 1992; Chen et al., 1995). The well-known quenching of Trp fluorescence by His (Shinitzky and Goldman, 1967; Willaert and Engelborghs, 1991) might involve either charge transfer (Werner and Forster, 1979) or proton transfer mechanisms (Yu et al., 1992). Water quenching should marginally affect the Trp lifetime in the presence of an efficient nonradiative pathway such as electron transfer to the carbonyl group, because the quenching rate of NATA by water is only $3.4 \times 10^7$ s$^{-1}$ (Chen et al., 1996). Photoionization, which might depend on the environment, arises from a prefluorescent state and thus leads to static quenching without affecting the lifetime (Mialocq et al., 1982). Intersystem crossing seems to be insensitive to protein functional groups (Chen et al., 1996).

Table 6 reports potential quencher groups within an 8-Å radius from the geometric center of the indole moiety. Except for the carbonyl groups of Glu-37 and Gln-38, all other potential quenchers are within 6 Å from at least one atom of the indole moiety. Because the charge transfer rate depends on orbital overlapping (Hopfield, 1977), the dis-

**TABLE 6 Potential quencher groups within 8 Å of the Trp-43 geometric center**

| Rotamer | Potential quencher groups | Distances to indole center (Å)* |
|---|---|---|
| I | Pro-39:C=O | 7.39 |
| (−170°, −80°) | Thr-40:C=O | 6.64 |
| | Leu-41:C=O | 7.76 |
| | Tyr-42:C=O | 6.60 |
| | Trp-43:C=O | 4.34 |
| | His-44:C=O | 7.44 |
| | His-44:imidazolering | 5.58 |
| | Lys-46:N$^\zeta$ | 6.32 |
| | | |
| II | Pro-39:C=O | 6.72 |
| (−170°, 80°) | Thr-40:C=O | 6.77 |
| | Tyr-42:C=O | 6.46 |
| | Trp-43:C=O | 4.93 |
| | His-44:imidazolering | 6.77 |
| | Lys-46:N$^\zeta$ | 6.48 |
| | | |
| III | Glu-37:C=O | 7.83 |
| (−70°, 160°) | Gln-38:C=O | 7.30 |
| | Pro-39:C=O | 3.98 |
| | Thr-40:C=O | 4.73 |
| | Leu-41:C=O | 6.88 |
| | Tyr-42:C=O | 6.46 |
| | Trp-43:C=O | 6.23 |
| | His-44:imidazolering | 6.71 |

*Distances are measured from the geometric center of the indole moiety to the geometric center of the C=O bond and of the imidazole ring and to the N$^\zeta$ atom of Lys-46.

tance to the closest carbonyl should be crucial for lifetime values. Table 5 clearly shows that rotamer III is closer to peptidic carbonyl groups than are the other two rotamers. The center of rotamer III is 3.98 Å from the C=O group of Pro-39, the shortest distance observed. A second carbonyl group (Thr-40) is within 5 Å of the center of the indole moiety. In addition, the $C^{\delta 1}$ and $C^{\delta 2}$ atoms of rotamer III are, respectively, 3.18 and 3.57 Å from the oxygen atom of Pro-39. They can easily encounter it upon librational motion about the $C^{\alpha}$-$C^{\beta}$ ($C^{\delta 1}$) or $C^{\beta}$-$C^{\gamma}$ ($C^{\delta 2}$) bonds, which should lead to very efficient deexcitation by charge transfer, whereas the *trans* rotamers cannot contact carbonyl groups. This strongly suggests that the subnanosecond component can be attributed to rotamer III.

The two *trans* rotamers are not equivalent with regard to quencher groups. In both cases, the closest carbonyl group is that of Trp-43. However, the distance of the indole barycenter to Trp-43 carbonyl is shorter for rotamer I (4.34 Å) than rotamer II (4.93 Å). In addition, there are six and four carbonyl groups within an 8-Å radius from the barycenter of rotamers I and II, respectively. Lys-46:$N_{\zeta}$ is at similar distance for both *trans* rotamers. The imidazole ring of His-44 is markedly closer to rotamer I (5.58 Å) than to rotamer II (6.77 Å), allowing interaction in the former case and not in the latter one. This strongly suggests that rotamer I could be related to the middle-lived component, whereas rotamer II would be related to the longest component. This assignment agrees well with our preliminary anisotropy study (Chabbert et al., 1992), because the steady-state anisotropy of rotamer I should be significantly higher than that of rotamer II, because of a smaller amplitude of librational motion (higher $r_{t=0}$) and shorter lifetime. Rotamer IV has not been taken into account because of its negligible weight as compared to the other rotamers. It is noteworthy, however, that because of its proximity to Pro-39:O (closest distance 2.95 Å), its lifetime should be very short.

There is a very satisfying correlation between the most probable rotamer positions and fluorescence lifetimes. Quantitative disagreement between rotamer distribution and preexponential terms can arise from several factors: 1) the concentrations of lifetime-defined species may be different from lifetime preexponential terms at the emission maximum, because of different decay-associated spectra and/or molar extinction coefficients; 2) in addition to molecular mechanics limitations due to, e.g., solvent representation, minimized energy mapping studies arise from a static picture of the protein structure, with complete relaxation of the environment around each Trp dihedral position. This is not realistic within a dynamic model of the protein structure. Better estimates of the Trp-43 $\chi_1 \times \chi_2$ isomerization space and relative rotamer populations would require dynamic simulations.

Each rotamer experiences librational, wobbling, and segmental motions. Backbone wobbling and DNA binding domain segmental motions are the same for each rotamer, whereas the amplitude of librational motions about the $C^{\alpha}$-$C^{\beta}$ and the $C^{\beta}$-$C^{\gamma}$ bonds are different. As the librational

motion time scale is much lower than the shortest lifetime, the observed ultrafast order parameter corresponds to the relative concentration-weighted average of the individual ultrafast order parameters and is consistent with the size of the wells. This corroborates the nonassociative model used for anisotropy decay analysis.

## Conformational changes induced by AnTc binding

AnTc binding to F75 TetR induces a marked change in the preexponential factors of the decay components (Table 1). In addition, there is a significant decrease in the long lifetime. Within the framework of the rotamer model, these changes in the Trp-43 fluorescence decay parameters upon AnTc binding indicate that 1) AnTc binding alters the rotamer distribution of Trp-43, favoring the rotamer corresponding to the middle lived component; 2) AnTc binding alters the nonradiative decay rate of rotamer II. This strongly suggests local structural changes in the DNA-binding domain upon inducer binding, in addition to the motion of this domain relative to the core of the protein.

The side chains nearest to Trp-43 rotamer II are His-44 and Lys-46. His-44 is at the C-terminal position of helix-3, and Lys-46 is in the loop joining helix-3 to helix-4. In the crystal structure, the position of Lys-46 is stabilized by a H bond between Lys-46:$N^{\zeta}$ and Trp-43:O. Upon isomerization, the distance between Lys-46:$N^{\zeta}$ and the indole center can vary from less than 6 Å to more than 13 Å, leading to very different electrostatic environments of Trp-43. Motion of helix-4 upon inducer binding (Hinrichs et al., 1994; Kisker et al., 1995) would probably modify the positioning of Lys-46. A change in the position of the ε-amino group of Lys-46 could alter the nonradiative decay rate of rotamer II, either directly through an excited-state proton transfer mechanism (Yu et al., 1992) or indirectly through an effect on the solvent quenching rate (Yu et al., 1995).

Our results suggest that local structural changes in the vicinity of Trp-43 upon inducer binding might favor the Trp conformation interacting with His-44. A change in the position of Lys-46 due to helix-4 motion may alter the relative energies of the different rotamers, because of different electrostatic environments. Alternatively, helix-4 motion could modify the positioning of the N-terminal tail. In the complex with tetracycline, Arg-6 in helix-1 (mutated to type-conserved Lys in class B TetR) is hydrogen-bound to Arg-104 in the core of the protein and to Asp-53 in helix-4 through a network of structurally important water molecules (Kisker et al., 1995). This network contributes to the stability and the positioning of the N-terminal tail and should be altered upon inducer removal, which modifies the relative positions of the DNA binding domain, the helix-4, and the repressor core. His-44 is stuck between rotamer I and the carbonyl oxygen of Leu-4. A different positioning of the tail would alter His-44 and Trp-43 rotamer I constraints and, thus, the energy of this rotamer for entropic reasons. This is

consistent with our preliminary study on Trp-43 (Chabbert et al., 1992), which showed that, for free repressor, the equilibrium between the different decay components was entropy driven.

In conclusion, our results on TetR Trp-43 fluorescence can be explained within the framework of the "rotamer model." The three fluorescence decay components can be related to three different rotameric orientations of the Trp side chain. Because of the asymmetry of the indole ring, both $\chi_1$ and $\chi_2$ rotamers have distinct environments and differential positions relative to carbonyl groups and side chains. In the present study, the backbone conformation is determinant for the position of the isomerization minima, because of the "exposed" location of Trp-43 (Dunbrack and Karplus, 1994). Generally, packing requirements at the tertiary structure level can alter side-chain orientation, and the stable rotamer positions will depend upon specific and local tertiary interactions. Isomerization mapping is clearly useful for rotamer search and correlation of the time-resolved fluorescence decay of a Trp residue with the local structure of its environment. The understanding of the time-resolved fluorescence and anisotropy parameters of the Trp residue in conformational and dynamic terms will increase its usefulness as a local probe of protein structure and motion.

# REFERENCES

Alcala, J. R., E. Gratton, and F. G. Prendergast. 1987. Interpretation of fluorescence decays in proteins using continuous lifetime distributions. *Biophys. J.* 51:925–936.

Alexandrescu, A. T., and D. Shortle. 1994. Backbone dynamics of a highly disordered 131 residue fragment of staphylococcal nuclease. *J. Mol. Biol.* 242:527–546.

Armstrong, K. M., R. Fairman, and R. L. Baldwin. 1993. The (i, i + 4) Phe-His interaction studied in an alanine-based a-helix. *J. Mol. Biol.* 230:284–291.

Bajzer, Z., and F. Prendergast. 1993. A model for multiexponential tryptophan fluorescence intensity decay in proteins. *Biophys. J.* 65: 2313–2323.

Beechem, J. M. 1992. Global analysis of biochemical and biophysical data. *Methods Enzymol.* 210:37–54.

Beechem, J. M., and L. Brand. 1985. Time-resolved fluorescence of proteins. *Annu. Rev. Biochem.* 54:43–71.

Berman, H. A., J. Yguerabide, and P. Taylor. 1980. Fluorescence energy transfer on acetylcholinesterase: spatial relationship between peripheral site and active center. *Biochemistry.* 19:2226–2235.

Bevington, P. R. 1969. Data Reduction and Error Analysis for the Physical Sciences. McGraw-Hill, New York.

Chabbert, M., W. Hillen, D. Hansen, M. Takahashi, and J. A. Bousquet. 1992. Structural analysis of the operator binding domain of Tn10-encoded Tet repressor: a time-resolved fluorescence and anisotropy study. *Biochemistry.* 31:1951–1960.

Chen, C., Y. Feng, J. Short, and J. Wand. 1993. The main chain dynamics of a peptide bound to calmodulin. *Arch. Biochem. Biophys.* 306: 510–514.

Chen, R. F., J. R. Knutson, H. Ziffer, and D. Porter. 1991. Fluorescence of tryptophan dipeptides: correlations with the rotamer model. *Biochemistry.* 30:5184–5195.

Chen, Y., B. Liu, and M. D. Barkley. 1995. Trifluoroethanol quenches indole fluorescence by excited-state proton transfer. *J. Am. Chem. Soc.* 117:5608–5609.

Chen, Y., B. Liu, H.-T. Yu, and M. D. Barkley. 1996. The peptide bond quenches indole fluorescence. *J. Am. Chem. Soc.* 118:9271–9278.

Clore, G. M., P. C. Driscoll, P. T. Wingfield, and A. M. Gronenborn. 1990. Analysis of the backbone dynamics of interleukin-1β using two-dimensional inverse detected heteronuclear $^{15}N$-$^1H$ NMR spectroscopy. *Biochemistry.* 29:7387–7401.

Colucci, W. J., L. Tilstra, M. C. Sattler, F. R. Fronczek, and M. D. Barkley. 1990. Conformational studies of a constrained tryptophan derivative: implications for the fluorescence quenching mechanism. *J. Am. Chem. Soc.* 112:9182–9190.

Cross, A. J., and G. R. Fleming. 1984. Analysis of time-resolved fluorescence anisotropy decays. *Biophys. J.* 46:45–56.

Dahms, T. D., K. J. Willis, and A. G. Szabo. 1995. Conformational heterogeneity of tryptophan in a protein crystal. *J. Am. Chem. Soc.* 117:2321–2326.

Dale, R. E., J. Eisinger, and W. E. Blumberg. 1979. The orientational freedom of molecular probes. The orientation factor in intramolecular energy transfer. *Biophys. J.* 26:161–194.

Dauber-Osguthorpe, P., V. A. Roberts, D. J. Osguthorpe, J. Wolff, M. Genest, and A. T. Hagler. 1988. Structure and energetics of ligand binding to proteins: *Escherichia coli* dihydrofolate reductase-trimethoprim, a drug-receptor system. *Proteins Struct. Funct. Genet.* 4:31–47.

Degenkolb, J., M. Takahashi, G. A. Ellestad, and W. Hillen. 1991. Structural requirements of tetracycline-Tet repressor interaction: determination of equilibrium binding constants for tetracycline analogs with Tet repressor. *Antimicrob. Agents Chemother.* 35:1521–1590.

Dezube, B., C. M. Dobson, and C. E. Teague. 1981. Conformational analysis of tryptophan in solution using nuclear magnetic resonance methods. *J. Chem. Soc. Perkin Trans.* 2:730–735.

Dunbrack, R. L., and M. Karplus. 1994. Conformational analysis of the backbone-dependent rotamer preferences of protein sidechains. *Nature Struct. Biol.* 1:334–340.

Förster, Th. 1948. Zwischenmolekulare Energiewanderung und Fluoreszenz. *Ann. Phys.* 2:55–75.

Hansen, D., L. Altschmied, and W. Hillen. 1987. Engineered Tet repressor mutants with single tryptophan residues as fluorescent probes. *J. Biol. Chem.* 262:14030–14035.

Haydock, C. 1993. Protein side chain rotational isomerization: a minimum perturbation mapping study. *J. Chem. Phys.* 98:8199–8214.

Hillen, W., and C. Berens. 1994. Mechanisms underlying expression of Tn10 encoded tetracycline resistance. *Annu. Rev. Microbiol.* 48: 345–369.

Hinrichs, W., C. Kisker, M. Düvel, A. Müller, K. Tovar, W. Hillen, and W. Saenger. 1994. Structure of the Tet repressor-tetracycline complex and regulation of antibiotic resistance. *Science.* 264:418–420.

Hopfield, J. J. 1977. Photo-induced charge transfer. A critical test of the mechanism and range of biological electron transfer processes. *Biophys. J.* 18:311–321.

Ichiye, T., and M. Karplus. 1983. Fluorescence depolarization of tryptophan residues in proteins: a molecular dynamics study. *Biochemistry.* 22:2884–2893.

Kisker, C., W. Hinrichs, K. Tovar, W. Hillen, and W. Saenger. 1995. The complex formed between Tet repressor and tetracycline-$Mg^{2+}$ reveals mechanism of antibiotic resistance. *J. Mol. Biol.* 247:260–280.

Lami, H., and E. Piémont. 1992. Fluorescence decay analysis by iterative reconvolution based on the estimated covariance matrix. *Chem. Phys.* 163:149–159.

Lipari, G., and A. Szabo. 1980. Effect of librational motion on fluorescence depolarization and nuclear magnetic resonance relaxation in macromolecules and membranes. *Biophys. J.* 30:489–506.

Lipari, G., and Szabo, A. 1982. Model-free approach to the interpretation of nuclear magnetic resonance relaxation in macromolecules. 2. Analysis of experimental results. *J. Am. Chem. Soc.* 104:4559–4570.

Loewenthal, R., J. Sancho, and A. R. Fersht. 1992. Histidine-aromatic interactions in Barnase. Elevation of histidine $pK_a$ and contribution to protein stability. *J. Mol. Biol.* 224:759–770.

Machado, F. C., C. Demicheli, A. Garnier-Suillerot, and H. Beraldo. 1995. Metal complexes of anhydrotetracycline. 2. Absorption and circular dichroism study of Mg(II), Al(III), and Fe(III) complexes. Possible influence of the Mg(II) complex on the toxic side effects of tetracycline. *J. Inorg. Biochem.* 60:163–173.

Mandel, A. M., M. Akke, and A. G. Palmer, III. 1995. Backbone dynamics of *Escherichia coli* ribonuclease HI: correlations with structure and function in an active enzyme. *J. Mol. Biol.* 246:144–163.

Mialocq, J. C., E. Amouyal, A. Bernas, and D. Grand. 1982. Picosecond laser photolysis of aqueous indole and tryptophan. *J. Phys. Chem.* 86:3173–3177.

Petrich, J. W., M. C. Chang, D. B. McDonald, and G. R. Fleming. 1983. On the origin of nonexponential fluorescence decay in tryptophan and its derivatives. *J. Am. Chem. Soc.* 105:3824–3832.

Peviani, C., W. Hillen, N. Ettner, H. Lami, S. M. Doglia, E. Piémont, C. Ellouze, and M. Chabbert. 1995. Spectroscopic investigation of Tet repressor tryptophan-43 upon specific and nonspecific DNA binding. *Biochemistry.* 34:13007–13015.

Phillips, L. A., S. P. Webb, S. J. Martinez, III, G. R. Fleming, and D. H. Levy. 1988. Time-resolved spectroscopy of tryptophan conformers in a supersonic jet. *J. Am. Chem. Soc.* 110:1352–1355.

Ponder, J. W., and F. M. Richards. 1987. Tertiary templates for proteins. Use of packing criteria in the enumeration of allowed sequences for different structural classes. *J. Mol. Biol.* 193:775–791.

Ricci, R. W. 1970. Deuterium-isotope effect on the fluorescence yields and lifetimes of indole derivatives-including tryptophan and tryptamine. *Photochem. Photobiol.* 12:67–75.

Ricci, R. W., and J. M. Nesta. 1976. Inter- and intramolecular quenching of indole fluorescence by carbonyl compounds. *J. Phys. Chem.* 80:974–980.

Ross, J. B. A., H. R. Wyssbrod, R. A. Porter, G. P. Schwartz, C. A. Michaels, and W. R. Laws. 1992. Correlation of tryptophan fluorescence intensity decay parameters with ¹H NMR-determined rotamer conformations: [tryptophan2]oxytocin. *Biochemistry.* 31:1585–1594.

Schnarr, M., M. Matthies, and W. Lohmann. 1979. The influence of different solvents on the interaction between metal ions and tetracycline. *Z. Naturforsch.* 34c:1156–1161.

Schrauber, H., F. Eisenhaber, and P. Argos. 1993. Rotamers: to be or not to be? An analysis of amino acid side-chain conformations in globular proteins. *J. Mol. Biol.* 230:592–612.

Shinitzky, M., and R. Goldman. 1967. Fluorometric detection of histidine-tryptophan complexes in peptides and proteins. *Eur. J. Biochem.* 3:139–144.

Silva, N. D., and F. G. Prendergast. 1996. Tryptophan dynamics of the FK506 binding protein: time-resolved fluorescence and simulations. *Biophys. J.* 70:1122–1137.

Skrabal, P., V. Rizzo, A. Baici, F. Bangerter, and P. L. Luisi. 1979. Co-oligopeptides containing two aromatic residues spaced by glycyl residues. X. Proton magnetic resonance study of co-oligo peptides of tryptophan and glycine. *Biopolymers.* 18:995–1008.

Szabo, A. G., and D. M. Rayner. 1980. Fluorescence dacay of tryptophan conformers in aqueous solution. *J. Am. Chem. Soc.* 102:554–563.

Takahashi, M., L. Altschmied, and W. Hillen. 1986. Kinetic and equilibrium characterization of the Tet repressor-tetracycline complex by fluorescence measurements. *J. Mol. Biol.* 187:341–348.

Vix, A., and H. Lami. 1995. Protein fluorescence decay: discrete components or distribution of lifetimes? Really no way out of the dilemma? *Biophys. J.* 68:1145–1151.

Weaver, A. J., M. D. Kemple, and F. G. Prendergast. 1989. Characterization of selectively ¹³C-labeled synthetic melittin and melittin analogues in isotropic solvents by circular dichroism fluorescence, and NMR spectroscopy. *Biochemistry.* 28:8624–8639.

Werner, T. C., and L. S. Forster. 1979. The fluorescence of tryptophyl peptides. *Photochem. Photobiol.* 29:905–909.

Willaert, K., and Y. Engelborghs. 1991. The quenching of tryptophan fluorescence by protonated and unprotonated imidazole. *Eur. Biophys. J.* 20:177–182.

Yamamoto, Y., and J. Tanaka. 1972. Polarized absorption spectra of crystals of indole and its related compounds. *Bull. Chem. Soc. Jpn.* 65:1362–1366.

Yu, H.-T., W. J. Colucci, M. L. McLaughlin, and M. D. Barkley. 1992. Fluorescence quenching in indoles by excited-state proton transfer. *J. Am. Chem. Soc.* 114:8449–8454.

Yu, H.-T., M. A. Vela, F. R. Fronczek, M. L. McLaughlin, and M. D. Barkley. 1995. Microenvironmental effects on the solvent quenching rate in constrained tryptophan derivatives. *J. Am. Chem. Soc.* 117:348–357.